Liner multiphysics coupling between grazing flow, thermal gradients, and sound pressure levels

Victor Lafont, Fabien Méry, Frank Simon

Liner multiphysics coupling between grazing flow, thermal gradients and high sound pressure levels

Victor Lafont*, Fabien Méry† and Frank Simon‡
ONERA/DMPE - Toulouse University , F-31055, Toulouse, France

The evolution of turbofan engines has led to designs with larger fan diameters, shorter inlets and thinner nacelle walls. This has forced the acoustic liners used therein to be placed closer to engine components that undergo significant thermal heating. This experimental study investigates the combined effects of important thermal gradients, grazing flow and acoustic level on liners applied to the LEONAR (Long Elastic Open Neck Acoustic Resonator) liner concept. Previous studies have shown that a coupling between these three effects can exist. The objective is to compare such a liner concept to a classical equivalent SDOF liner and to highlight differences in this coupling behavior . Experiments are conducted in the grazing flow duct at ONERA (B2A) where the flow temperature can be accurately regulated and several types of acoustic excitation can be provided. A test section with a heating or cooling device is used to obtain a thermal gradient between the backplate and the perforated plate of the liner sample, and infrared thermography is used to measure the temperature distribution on the perforated plate. The measurement is conducted on several configurations to assess the behaviors of the LEONAR liner concept in the context of combined influence of grazing flow, thermal gradients and high sound levels.*

Nomenclature

ϕ	=	Liner perforated sheet perforation diameter (mm)
δ	=	Liner perforated sheet thickness (mm)
l_t	=	Length of extended necks under perforate sheet (mm)
L_s	=	Sample thickness (m)
ρ_0	=	Density of the mean flow (kg/m^3)
M_b	=	Grazing flow bulk Mach number
q_m	=	Mass flow rate (g/s)
ω	=	Angular frequency (rad/s)
ζ	=	Normalized acoustic impedance
r	=	Normalized acoustic resistance (real part of ζ)
χ	=	Normalized acoustic reactance (imaginary part of ζ)
a	=	B2A cross section height (mm)
S	=	B2A cross section area (mm^2)
(x, y, z)	=	Axial, transversal and vertical coordinates (mm)
c_0	=	Speed of sound in air (m/s)

*Phd student, victor.lafont@onera.fr
†Research Scientist, fabien.mery@onera.fr
‡Research Scientist, frank.simon@onera.fr
*This work has been presented at AIAA AVIATION FORUM 2021, August 2-6 2021, Virtual event, Paper AIAA 2021-2204

k_{body} = Sample thermal conductivity ($\text{W.m}^{-1}.\text{K}^{-1}$)
Bi = Biot number
h = Convective heat transfer coefficient ($\text{W.m}^{-2}.\text{K}^{-1}$)
T_{flow} = Grazing flow static temperature (°C)
T_u = Perforated plate adiabatic temperature (°C)
T_b = Backplate temperature (°C)

I. Introduction

With the development of UHBR (Ultra High Bypass Ratio) engines optimized for maximum propulsion efficiency, new challenges arise regarding the implementation of conventional noise-absorbing liners. Indeed, the thinner and shorter nacelles leave less room to accommodate acoustic liners, whereas these same liners need to increase in height in order to properly absorb the lower-frequency noise generated by a larger fan. Moreover, the thinner walls between the combustion chamber and the bypass ducts will be likely to induce thermal gradients inside the liners' structure itself. Therefore, there is a growing need to propose new liner concepts that deal with these challenges. These concepts must be characterized as precisely as possible and their behavior must be assessed when thermal gradients, complex flows and high noise levels are involved simultaneously.

Conventional, single degree of freedom (SDOF) liners consist of a honeycomb structure topped with a thin perforated facesheet, forming a layout of small resonators closed at their bottom by a rigid backplate. The geometry of the honeycomb can be adjusted to match specific noise damping requirements [1]. The driving parameter for the noise damping power of "locally reacting" liners is their acoustic impedance, a complex number that is the ratio between acoustic pressure p and normal acoustic velocity v_n taken on the facesheet, normalized by the impedance of air $\rho_0 c_0$:

$$\zeta(\omega) = \frac{Z(\omega)}{\rho_0 c_0} = \frac{p}{\rho_0 c_0 v_n} = r(\omega) + \mathrm{j}\chi(\omega),$$

where r and χ are respectively called the resistance and the reactance of the liner.

It is generally admitted that resistance can be increased by the sound pressure level (SPL) or by the grazing flow. These effects are so-called nonlinear effects linked to a vortex shedding produced periodically near the perforations [2]. Having a varying resistance due to SPL could be a drawback in terms of designing liner solutions . Several models for acoustic liners exist and take into account these effects. Guess [3], for instance, gave a solution to model the effect of SPL and grazing flow. It appears necessary to propose a solution that is, as much as possible, weakly nonlinear, for example, a liner with a thicker perforated plate so the nonlinear effects are slightly reduced (because of a high ratio between the perforated plate thickness δ and the hole diameter ϕ [4, 5]). This solution is acoustically efficient, but the thicker plate cannot be an acceptable solution in terms of liner mass. Similarly, the total height of the cavity is a driving parameter for the frequency selection: to absorb at lower frequencies, a higher cavity is required. Again, this is not fully compatible with aeronautical constraints in the UHBR context. The LEONAR concept (or HREN for Helmholtz Resonator with Extended Neck) [6–8] could be a good candidate to cope with these challenges. It consists in linking the perforated layer with hollow tubes introduced in the honeycomb, to shift resonance frequencies to lower frequencies by a prolongation of air column lengths. Recently, Guo et al. [9] proposed the design of an optimal liner constructed by 16 inhomogeneous HRENs, allowing to have a sound absorption in a prescribed frequency range from 700 to 1000 Hz. The same authors applied this concept to a small-scale propeller [10] where the liner concept has to be very compact regarding the available space. These types of liner concepts are thus very interesting in order to design an optimal liner for a given application.

Thermal conditions also affect the impedance of liners. Elnady et al. [11] investigated the acoustic behavior of a

single orifice over a cavity placed in an oven. The surface of the sample was hotter than the back of the cavity, with a temperature difference up to 100 K. The measurements were conducted for several SPLs, including the nonlinear regime, but without any grazing flow. The impedance of the liner was measured with an in-situ technique and compared to existing semi-empirical models. It was found that an increase in temperature results in a decrease of the reactance, while the resistance slightly increases (at least when the nonlinear effects are small compared to the viscous ones). Modifying the properties of air in the model to account for the high temperatures appeared to be enough to predict quite well this impedance change; the decrease of the reactance is indeed due to the modification of the air density that impacts the speed of sound inside the cavity.

The coupling between aerodynamic and acoustic effects is complex, as liners increase the viscous drag in the turbulent layer compared to a smooth surface. Howerton et al. [12] investigated the drag effect of several conventional or more advanced liner designs in the NASA GFIT. They found that the resistance factor λ (also known as the friction factor) was frequency-dependent in the presence of acoustic excitation. This effect increased with SPL, but was mitigated at higher flow speeds. More recently, Jasinski et al. [13] highlighted that a dramatic increase in drag at frequencies near acoustic resonance and at high SPL is observed on classical SDOF liners. Zhang and Bodony [2] confirmed that high acoustic levels increased the liner drag by performing a series of Direct Numerical Simulations (DNS) reproducing the conditions of a single orifice-over-cavity liner undergoing a grazing flow. Leon et al. [14] used a high-magnification PIV setup to obtain 2D acoustic velocity fields measured close to the perforations of a SDOF liner sample. They observed that high acoustic levels induced specific aerodynamic phenomena and that the "rough-wall" analysis was showing its limits to predict the effects on the drag.

Giachetti et al. [15] experimentally studied the influence of synthetic pulsating jets across a multi-perforated wall. They studied the role of cross-flow and synthetic jet interactions and the effect on the convective thermal coefficient. It was the first experimental set up that enabled an understanding of the types of coupling between grazing flow, acoustic excitation and thermal gradients in acoustic liners. A numerical restitution of the previous experiment was proposed by Esnault [16]. Méry et al. [17] conducted a study on liner samples heated from the back wall, both with and without the presence of a cooler grazing flow. The acoustic response of the samples was investigated both in the linear and nonlinear regimes with respect to the acoustic level. They showed that the temperature changes mainly impacted the reactance as the sound speed inside the cavities was modified. The work also highlighted the influence of the acoustic level on the temperature distribution : for high SPL, the temperature went down inside the cavity due to the sample entering the nonlinear regime. This highlighted strong multiphysical coupling between the acoustics, flow and thermal phenomena. This was especially true of the nonlinear effect due to the SPL on the surface temperature and the thermal exchanges, as highlighted in Lafont et al. [18].

In this study, a multiphysics assessment will be performed on a LEONAR liner concept and insights will be given on its use in the UHBR context. This concept is compared to an acoustically equivalent SDOF liner. A specific experimental setup is designed and used to monitor precisely the evolution of a liner surface temperature when there is a thermal gradient inside it and in presence of high SPL. The measurements are conducted both with a hot and cool grazing flow and the experimental conditions are carefully controlled. In particular, the temperature is monitored in several locations all along the measurement. Impedance eduction is performed based on [19].

The objective of this study is to highlight the differences, in terms of impedance and thermal effects, between two liners that should have a similar acoustic behavior. The LEONAR concept enables a reduction of the total height of a given liner concept, thus reducing the overall mass. The impact of this architecture on the thermal ditribution and the impedance evolution in presence of a grazing flow and a thermal gradient needs to be assessed. The first part of this paper will be dedicated to the liner definition, the experimental methods and the setup. The second part will address impedance eduction results on two liner concepts. Finally, thermography results on the skin surface liner will be

presented and discussed.

II. Experimental methods and setup

A. Sample description

Two samples are used in this study. One is a simple SDOF liner that has already been studied previously at ONERA[17] . The second one is a LEONAR, a type of liner where the perforations of the facesheet are connected to hollow tubes extending inside the cavities (see Fig. 1). This specific geometry allows one to increase the perceived thickness of the facesheet without modifying the total height of the liner [7], therefore leading to lower-band absorption and a very linear response with respect to incident SPL. The LEONAR sample is based on the geometry of the SDOF sample. Thus, the perceived thickness of the perforated sheet is the same but the total height is reduced. The LEONAR sample is expected to have similar acoustic characteristics but differ in the thermal and grazing flow behavior. The two samples are metallic samples obtained by additive manufacturing.

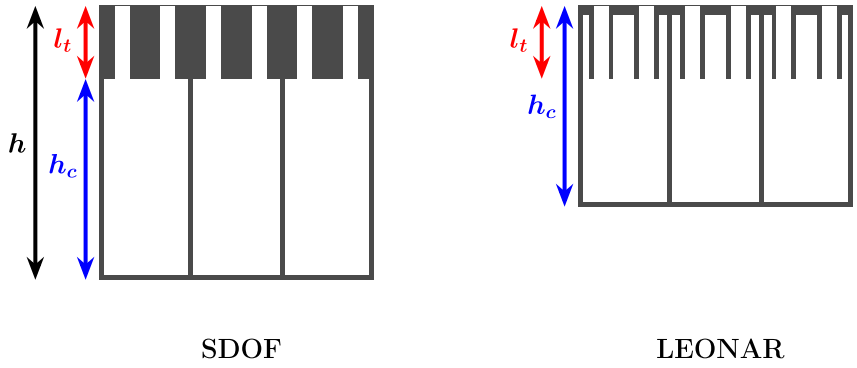

Fig. 1 Comparison of equivalent SDOF (left) and LEONAR (right). h_c is the inner cavity height, l_t the tube length (=δ for a SDOF sample)

Table 1 Geometric characteristics of the samples

Sample	ϕ (mm)	Porosity (POA)	l_t (mm)	Inner cavity height h_c (mm)	Total height h (mm)
SDOF	1.5	15%	8	41	50
LEONAR	1.5	15%	1 + 7	41	45

B. Acoustic setup

The B2A test bench is made of a stainless steel tube with a square section of side $a = 50$ mm and a total length of about 4 m. A mean flow of bulk Mach number M_b up to 0.5 can be provided and its temperature can be accurately regulated from room temperature up to 570 K. In the duct, the flow is in a fully-developed turbulent state, with axial velocity fluctuations on the centerline being a few percent of the bulk velocity U_b [14].

The parameter used to regulate the flow is the mass flow rate $q_m = \rho M_b c_0 S$ (in g/s), where $M_b = \frac{U_b}{c_0}$ is the bulk Mach number, $S = a^2$ is the duct cross-section, and c_0 is the sound speed in the duct. The flow temperature is also regulated. This regulation ensures that the conditions above the sample remain similar when the flow is heated or cooled. Table 2 shows the different flow rates used in this study and the corresponding bulk Mach numbers at different temperatures.

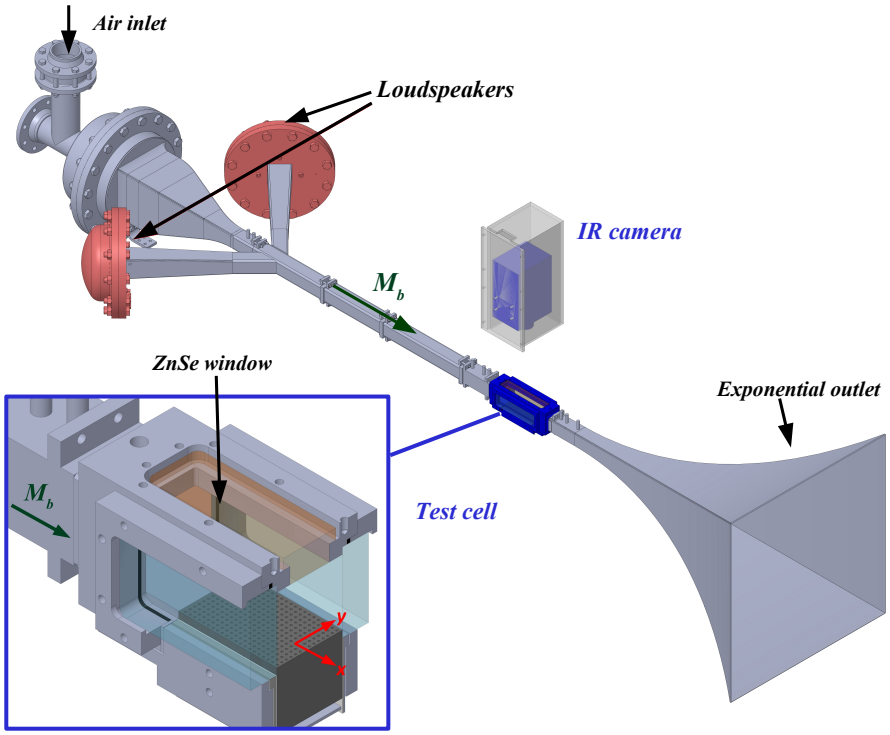

Fig. 2 The B2A bench

Table 2 Flow rates used and Mach numbers depending on the flow temperature

q_m (g/s)	M_b (T_{flow} = 20 °C)	M_b (T_{flow} = 87 °C)	M_b (T_{flow} = 117 °C)
50	0.048	0.054	0.056
100	0.097	0.107	0.112
150	0.145	0.161	0.168
200	0.194	0.215	0.224
260	0.251	0.278	0.290

The test section is 0.2 m-long and equipped with two opposing silica windows for optical access. An exponential quasi-anechoic outlet terminates the duct, leading to a reflection coefficient smaller than 0.2 for frequencies higher than 500 Hz. The surface of the test liner forms a 150 mm-long portion of the lower wall of the flow duct and spans all the duct width [20].

Sixteen microphone sockets in the upper wall of the test section are used for acoustic measurements and impedance eduction. The upper wall with the microphone sockets is removable and can be replaced by a window for infrared measurements. Silica windows on both sides allow near-wall optical measurements (LDV or PIV).

Upstream of the test section, two speakers are used to generate tones at up to 150 dB over a frequency range of 0.3 to 3.5 kHz (i.e. the no-flow cut-off frequency of the duct for plane waves). Mono-sine or multi-sine acoustic excitation can be used. The multi-sine is made of 12 pure tones ranging from 504 Hz to 2824 Hz (see Table 3) and of equal SPL, while the mono-sine is only a single pure tone. Multi-sine excitations are used to study global behaviors at low and medium SPLs while mono-sine excitations are used for studying the behavior at higher SPLs and at specific frequencies, for

example near the liner's resonance. When a multi-sine source is used, the overall SPL (OASPL) within the duct is much higher (usually 10 dB more) than the SPL at each tone frequency.

Table 3 Test Frequencies (the frequency used for mono-sine excitations is written in bold and red).

Frequencies (Hz)											
504	616	760	**992**	1112	1240	1488	1736	1992	2248	2488	2824

C. Thermal design and setup

Two distinct thermal configurations are used in this study. They are defined by the sign of the temperature difference $\Delta T = T_b - T_{flow}$ between the flow and the bottom of the liner. In the positive case, the bottom wall of the liner is heated and the flow at room temperature acts as a cold thermostat to obtain a thermal gradient in the sample. In the negative case, the flow is heated and the bottom wall is kept at a lower temperature to obtain a temperature gradient (Figs. 3 and 4).

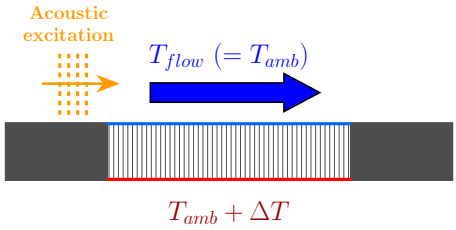

Fig. 3 Positive gradient

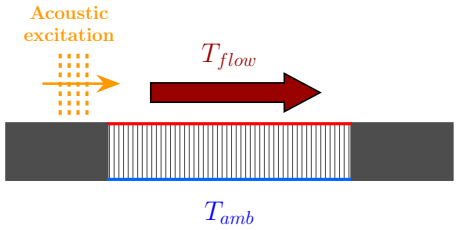

Fig. 4 Negative gradient

To ensure these two configurations can be obtained in a stable manner, a dedicated test cell has been designed (Fig. 5). It is partly based on the one developed for the study by Méry et al. [17] and can withstand high temperatures while remaining sealed and without undergoing significant thermal expansion. The sample holder has been designed to include as much thermal insulation as possible, so that significant thermal exchanges can only take place between the upper and lower walls of the sample and not on the four sides. The heating / cooling systems needed to obtain a thermal gradient are positioned under the sample and were designed to create thermal gaps between the backplate and flow up to 150 K. During the experiment, the flow temperature and the bottom temperature are monitored using type K thermocouples close to the inlet and on the backplate of the liner sample .

In the positive configuration, the bottom of the sample is heated by two electric resistors that are attached to the underside of a thin aluminum plate positioned just below the sample. In addition, the junction between the aluminum plate and the sample is sealed with thermal paste to ensure a good thermal conductivity. This setup ensures a homogeneous heating distribution. Figure 6 shows the sample holder with a liner mounted, seen from the bottom, with the resistors, the homogenizing aluminum plate and the various type K thermocouples used for temperature monitoring. The heating is regulated by an external system to maintain a constant given temperature on the bottom of the sample. This system combines a PID controller with a solid-state relay and works by controlling the resistors' power input to adjust the backplate temperature to match the target value T_b.

In the negative gradient configuration, the cooling of the sample's backplate is provided by circulating water through a metal block positioned under the sample. As with the heating plate, thermal paste is used at the junction between the block and the sample. Temperature regulation is obtained using a thermostatic bath that maintains a precise temperature and water flow rate. The water temperature is set to around 10 °C and the ideal water flow rate is determined by a 1D

preliminary calculation. If P_d is the power transmitted between the bottom of the sample and the outside, then:

$$P_d = \frac{T_u - T_b}{L_s/k_{\text{body}}} = h_{\text{water}} S_e (T_b - T_{\text{water}}) \tag{1}$$

where S_e is the total exchange area between the water and metal bloc and h_{water} is the corresponding convection heat coefficient. The water runs through tubes of diameter d_t drilled into the metal bloc, so h_{water} can be expressed as:

$$h_{\text{water}} = \text{Nu}\ \frac{k_{\text{water}}}{d_t} \tag{2}$$

where Nu is the Nusselt number and k_{water} is the thermal conductivity of water. The value of Nu is obtained through Colburn's correlation for a turbulent duct flow [21]:

$$\text{Nu} = 0.023 \times \text{Re}^{0.8} \times \text{Pr}^{1/3} \tag{3}$$

where Re and Pr are respectively the Reynolds and Prandtl numbers. For temperatures around 20 °C, we use $\text{Re} = 10^4 \times v_{\text{water}}$ where v_{water} is the water speed in m/s inside the tubes. The minimal flowspeed (in m/s) is then given by:

$$v_{\text{water}} = \left(\frac{P_d}{36.45 \times \text{Pr}^{1/3} \times \frac{k_{\text{water}}}{d_t} S_e (T_b - T_{\text{water}})} \right)^{\frac{1}{0.8}} \tag{4}$$

which, as we use three tubes ($d_t = 10$ mm) along the whole length of the sample, equals to a flow rate of around 3-5 L/min depending on the conditions of the air flow in the test section.

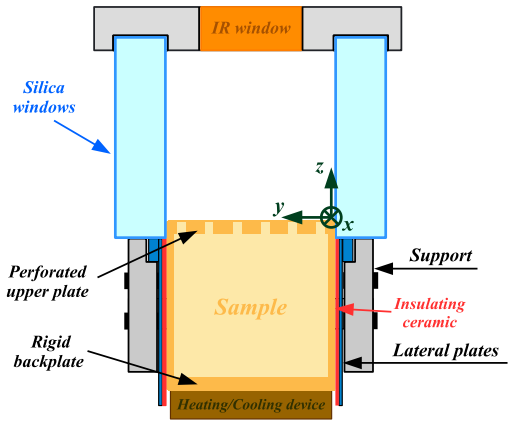

Fig. 5 Cross-section of the testing cell (facing downstream)

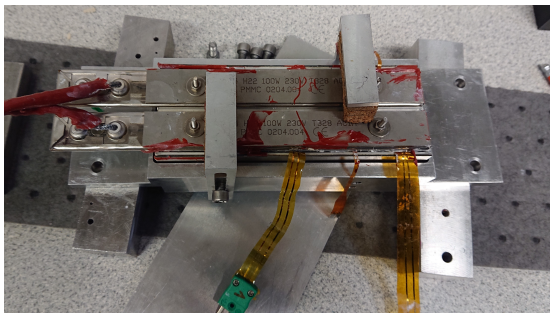

Fig. 6 Sample holder, liner sample and heating plate with complete instrumentation (seen from bottom)

D. Setup for infrared thermography

The temperature of the perforated plate T_u is obtained by infrared thermography (Fig. 7). Infrared (IR) thermography is a method of obtaining the temperature of a body by measuring the infrared radiation it emits. The technique relies on a good understanding of the physical phenomena involved and requires carefully controlled experimental conditions. An IR camera and a specific IR window with surface treatment adapted to transmit almost 100% of the incident infrared light are used. The IR window is placed in the top wall of the test section, allowing an overhead view of the sample's perforated facesheet. Two examples of raw infrared pictures are displayed in Figs. 8 and 9. The raw pictures have a

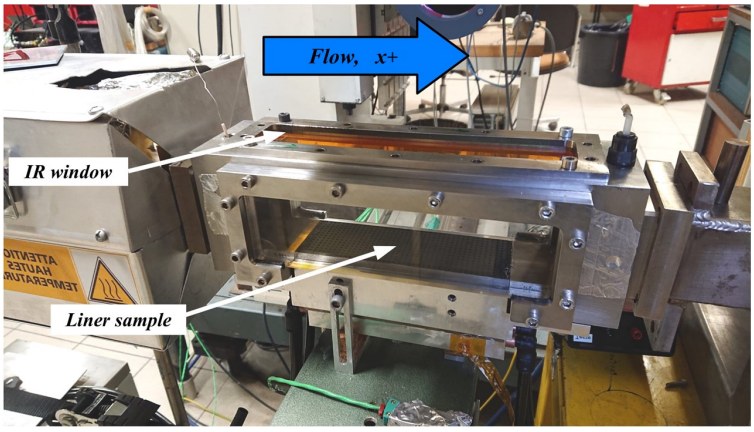

Fig. 7 B2A test section, with the cooling system (the flow and x axis go from left to right)

resolution of 640 pixels wide by 512 pixels high and a spatial resolution of approximately 4 pixels per millimeter . The camera is set up in order to have the area of interest centered in the picture, which minimizes the impact of distortion caused by the lens at the extremities. The camera's internal calibration law is established for several specific temperature ranges. In this study, the calibration used is valid for 15 °C < T_u < 73 °C .

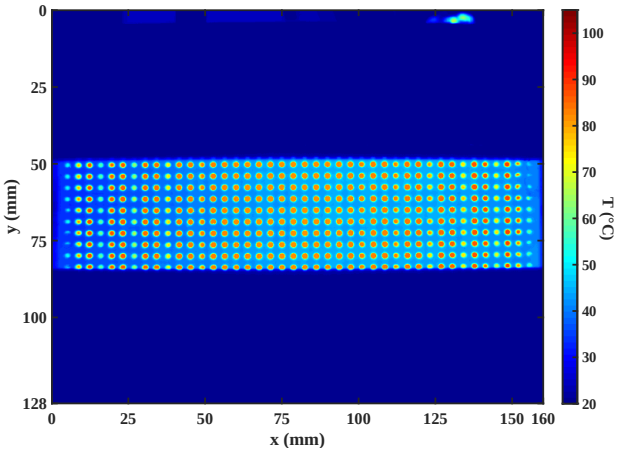

Fig. 8 Raw infrared picture, SDOF sample, q_m = 50 g/s, T_{flow} = 20 °C

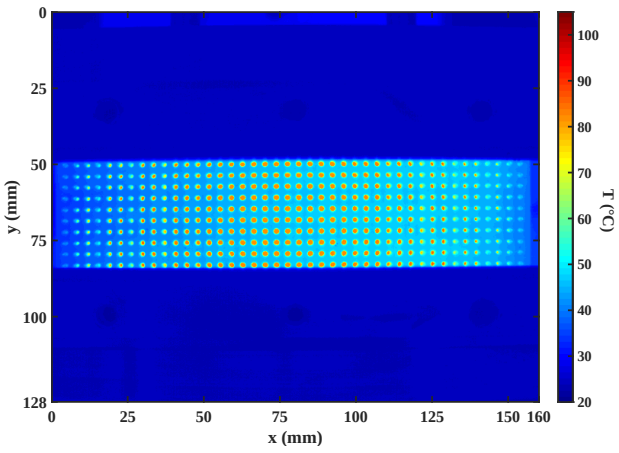

Fig. 9 Raw infrared picture, LEONAR sample, q_m = 50 g/s, T_{flow} = 20 °C

The sample have been painted with a specific paint with a high emissivity . An assessment of the complete setup's thermal stability was conducted using a plain rigid aluminum sample.

A complete analysis of the thermal features and the limitation of the set up was performed in a former study. The same post-processing procedure is applied in this article : the streamwise temperature profiles are obtained by removing the holes and averaging the temperature in the spanwise direction. Further details can be found in Lafont et al. [18]

III. Impedance and acoustic results

This section focuses on studying the acoustic behavior of the two liner samples in presence of grazing flow and thermal gradient. This is done on the B2A bench with the acoustic measurement techniques detailed in the previous section. The goal is to assess the similarities and discrepancies between the two samples regarding their acoustical properties and to evaluate the impact of grazing flow and thermal gradient on their respective impedances.

A. Transmission Loss

The global behavior of the samples is determined by measuring the transmission loss between upstream and downstream sections when the samples are mounted in the B2A test cell.

The incident acoustic wave p_i^I is a multi-sine set to 130 dB per tone. A two-microphone method [17, 22] is used to measure the acoustic pressures p_i and p_r in the upstream and downstream section (see Fig.10). The transmission loss in dB is then obtained by the ratio between the incident power and the transmitted power, since the downstream part ends into a quasi-anechoic termination, the reflection is assumed to be neglected relative to the incident power . As the frequencies used are below the cut-off frequency of the duct, only plane waves are considered and the incident and transmitted powers are directly linked to the SPL of p_i^I and p_i^{II}.

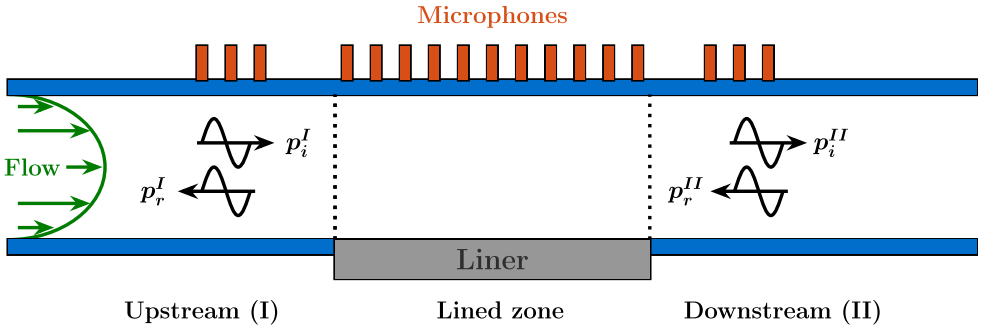

Fig. 10 Sketch of the measurement procedure

The transmission losses measured on the SDOF and LEONAR samples for $q_m = 100$ g/s are given in Figs. 11, 12 and 13. The optimal absorption band of the sample is the frequency band where the transmission loss is maximal. For the SDOF and LEONAR samples, this band is located around 1 kHz. The maximal TL values of these samples are close, and the width of the band is similar as well. The acoustic behavior of the LEONAR sample is thus very similar to the behavior of the SDOF. The TL is not significantly modified in presence of a thermal gradient. The main effect appears to be a slight shift of the maximum loss band towards higher frequencies, indicating a similar change in the resonance frequency. This slight shift can also be noticed for higher mass flow rate for the LEONAR liner This result is coherent with Mery et al. [17]: the shift is due to the variation of the temperature inside the cavity, which directly impacts the Helmholtz resonator characteristics.

B. Impedance eduction

The impedance of both samples is determined with an eduction method based on the two-dimensional time-harmonic linearized Euler equations (LEE).this is an iterative scheme whereby an assumed impedance is used in the LEE calculations to determine acoustic pressures at the microphone locations. This method relies on an iterative scheme whereby an assumed impedance is used in the LEE calculations to determine acoustic pressures at the microphone locations, as shown in Fig. 10.These pressures are compared to the experimental results until the assumed impedance minimizes the error between the two. The numerical resolution of the LEE is done with a discontinuous Galerkin (DG) scheme, accounting naturally for the presence of a shear grazing flow in the simulation [19, 23, 24].

Figures 14 to 17 show the impedance eduction results on both samples for $q_m = 100$ g/s and $q_m = 260$ g/s, with an incident SPL set to 130 dB per tone and for three thermal gradient conditions. The acoustic similarity between both samples appears clearly: their respective impedances have the same behavior over the considered frequency range, and their resonance frequencies (i.e. the frequency at which $\chi = 0$) are very close. The LEONAR liner type is assumed to be linear with respect to the SPL. [7].Regarding the SDOF with such a thick plate, an equivalent sample (same porosity,

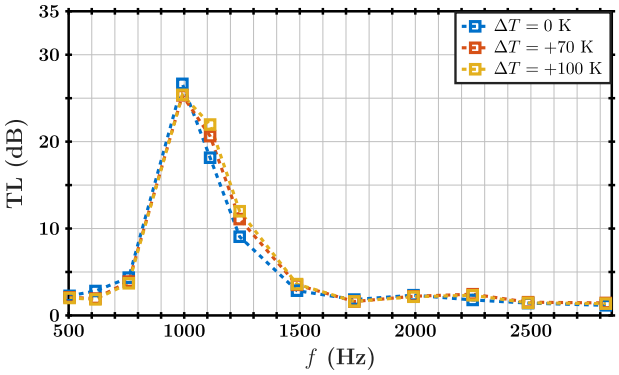

Fig. 11 Transmission Loss (TL), q_m = 100 g/s, sample SDOF

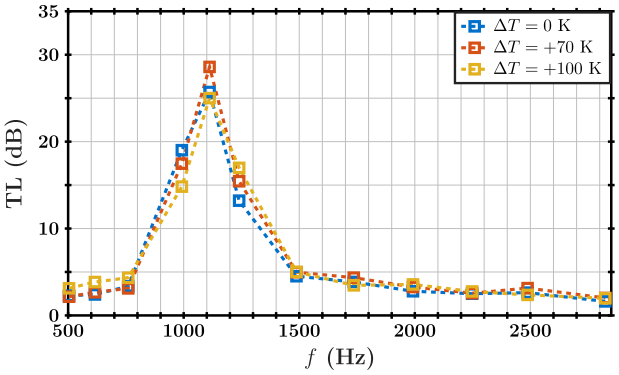

Fig. 12 Transmission Loss (TL), q_m = 100 g/s, sample LEONAR

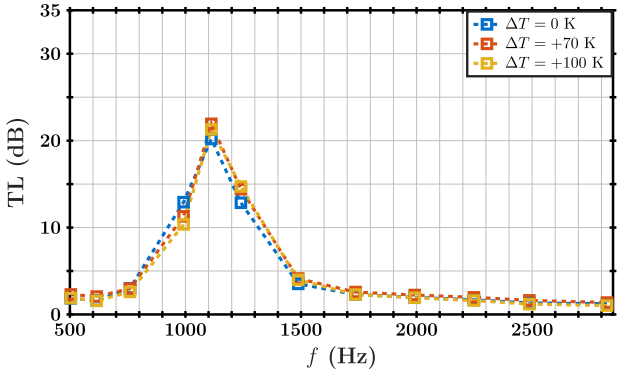

Fig. 13 Transmission Loss (TL), q_m = 260 g/s, sample LEONAR

same plate thickness, holes slightly smaller) has been tested in an impedance tube with increasing incident SPL and appeared to be linear regarding the SPL [17]. The influence of the grazing flow is visible and similar on both samples: the resistance r increases when q_m is greater.

Yang et al. [25] studied the variations of the impedance of several LEONAR-like liner samples when a grazing flow was applied. Using Guess's model [3] as a basis, they expressed the variation of the impedance taking into account the grazing flow Mach number and the end corrections for the extended tube. The variation of the resistance Δr linked to an increase of the grazing flow Mach number by ΔM_b is then expressed as:

$$\Delta r = \frac{K_M \Delta M_b}{\sigma} \tag{5}$$

where σ is the ratio between the tube and the cavity areas (equal to 0.18 for our LEONAR sample) and K_M is a constant of 0.12 according to Yang. This value is lower than the constant used in Guess's model, which is 0.3 for a SDOF liner; the effect of the grazing flow is expected to be less on a LEONAR liner than on a classical SDOF liner (in the sense of a thin perforated plate). Using the corresponding values of M_b in Table 2 and Equation 5, the increase of r when q_m varies from 100 to 260 g/s on the LEONAR sample should be equal to $\Delta r = 0.10$. Figure 18 shows a comparison between this predicted increase and the measured increase, taking in both cases the measured resistance at q_m = 100 g/s as a reference. Around the resonance of the liner (1 kHz), the agreement between the two values (r_p, orange squares , and r, blue squares) is quite good; but at higher frequencies (i.e. far from the resonance) the discrepancy increases. This was also noted by Yang et al. and attributed to higher uncertainties on the eduction procedure due to less acoustic

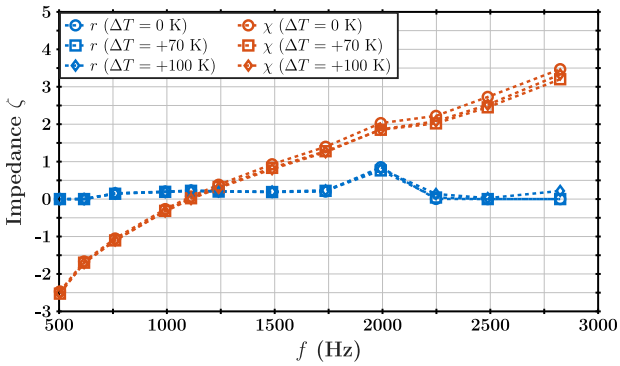

Fig. 14 LEONAR, q_m = 100 g/s

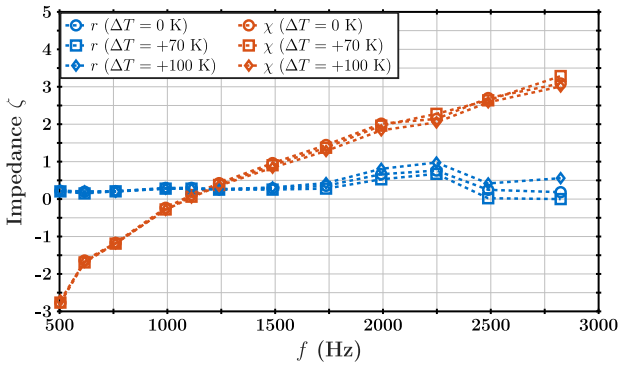

Fig. 15 LEONAR, q_m = 260 g/s

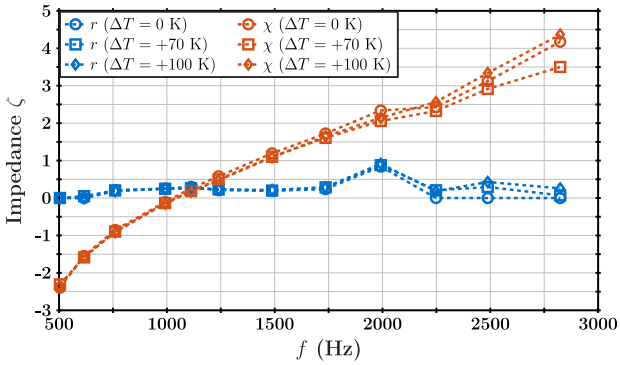

Fig. 16 SDOF, q_m = 100 g/s

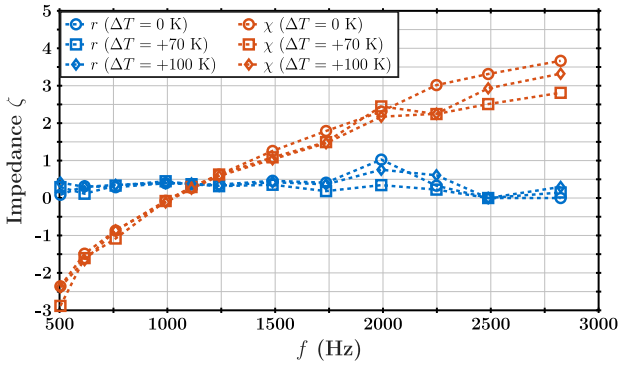

Fig. 17 SDOF, q_m = 260 g/s

absorption. Indeed, these liners have a very low resistance value, the eduction procedure generally fails to find the right value for the resistance. In the present case, for q_m = 100g/s over 2250Hz, the resistance is artificially found to be 0. It is thus impossible to conclude on the behavior at higher frequencies. On Figure 18,the model has not been applied on these higher frequencies.

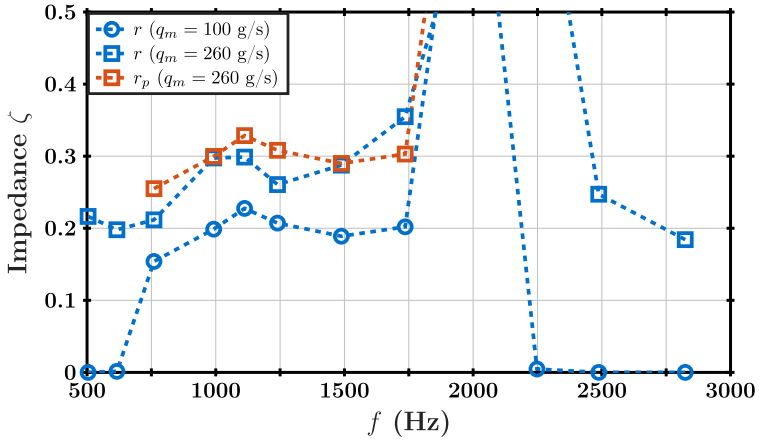

Fig. 18 Comparison of predicted (orange squares) and measured (blue squares) resistance increase at q_m = 260 g/s, taking the measured resistance at q_m = 100 g/s as a reference (blue circles)

On the other hand, the thermal conditions do not seem to affect much the resistance and the reactance of the two liners: the only significant and consistent effect is a slight shift of the resonance towards the higher frequencies

previously highlighted in [17]. This effect seems to be confirmed for the SDOF liner but is reduced on the LEONAR liner. The extended necks of the LEONAR sample apparently have an impact on the temperature distribution inside the cavities; this impact appears significant enough to counterbalance the effect of the thermal gradient on the reactance.

In [17], the main conclusion was that the reactance was modified due to the thermal gradient inside the cavity. In the case of a SDOF, a fair model was thus a classical perforated plate impedance model with grazing flow correction effect combined with a cavity impedance model considering an average temperature (an average between bottom and flow temperature) inside the cavity. Considering the LEONAR, the extended necks seem to have an impact on the temperature distribution inside the cavity and thus a temperature correction should be considered to model the impedance correctly. The grazing flow effect based on Yang's model seems to work. Finally, classical LEONAR models with grazing flow effect should give interesting more accurate results as long as the correct temperature inside the cavity is used. A thermocouple measure inside the sample should be performed in order to have a profile of the temperature inside the cavity and thus this ideal temperature.

IV. Thermal characterization results

The work by Giachetti et al. [15] and Esnault et al. [16] highlighted the influence of synthetic jets on the heat transfer coefficient of a heated perforated plate subjected to a grazing flow. Since the synthetic jets were emerging from the perforations, this configuration is very similar to our liner subjected to grazing flow, thermal gradients and an acoustic excitation that induces the synthetic jets; thus, similar couplings between aeroacoustic and thermal effects are expected. The goal is thus to assess the existence and intensity of the couplings between grazing flow, thermal and acoustic effects for each thermal configuration and each sample. This is achieved by comparing the surface temperatures of the liner with and without acoustic excitation, using a 1D-approach to link temperature variations to the heat transfer coefficient, following the methodology developed in [18].

A. Influence of liner type

Figures 19 through 22 show the measured surface temperature on SDOF and LEONAR liner samples at two different flow rates, with a positive thermal gradient defined by ΔT=+100 K. Three acoustic conditions are presented: without excitation, with a multi-sine excitation of SPL = 130 dB/tone, and with a single tone excitation near the resonance (992 Hz for both samples) of SPL = 140 dB. A fourth acoustic condition is also tested for the SDOF sample with a single tone at 1992 Hz (far from resonance) for q_m=50 g/s. The profiles are taken in the streamwise direction. The asymmetry of the streamwise profiles is explained by the thermal discontinuities that result in locally higher values of the convective heat transfer coefficient h. [18].

The surface temperature is lower on the LEONAR sample than on the SDOF sample in all cases. This is explained by the differences in their internal structures, which impacts their respective thermal conductivities. The equivalent thermal conductivity of the samples is indeed determined by taking into account the conductivity of the material of which they are made, and the conductivity of the air trapped inside the cavities. A different internal geometry, such as tubes in the case of the LEONAR sample, results in a different thermal conductivity and thus a different surface temperature. The model used in this study to compute the equivalent thermal conductivity is a simple geometrical approach, thus the values given should be taken with caution; however the values obtained for k_{body} (1.8 W.m^{-1}.K^{-1} for the SDOF sample and 1.1 W.m^{-1}.K^{-1} for the LEONAR sample) still give a coherent trend. Indeed, both samples have roughly the same cavity volume, but the LEONAR sample has less material and that material is also less conductive than the material used for the SDOF sample; therefore, the thermal conductivity of the LEONAR sample is lower than the conductivity of the SDOF sample.

Without any acoustic excitation (blue curves), the heat convection effect at the surface is visible on both samples. For

each sample, when the flow rate increases, the surface temperature decreases as the heat convection at the liner surface increases. The multi-sine acoustic excitation (red curves) leads to a decrease of the surface temperature. This effect is due to the increase of heat convection at the surface, caused by an interaction between the flow, the acoustic waves and the perforations. The reaction is a global one: the decrease is similar over the whole liner length. The temperature decrease is less important when q_m is higher, highlighting the competition between grazing flow and acoustic effects.

On the SDOF sample, when the acoustic excitation is a single tone with a frequency close to the resonance of the sample (yellow curves), the coupling phenomenon is significant . The surface temperature decreases a lot at the beginning of the liner but then increases gradually along the liner until it matches again the value in the case without acoustic excitation. This behavior is explained by the acoustic absorption along the sample: as the acoustic energy is absorbed, the SPL decreases and the aerothermal coupling with the acoustic behavior of the liner effect fades out. Indeed, this coupling effect is mainly due to the vortex-shedding phenomenon that increases the heat convection at the liner surface. This localized effect is not visible on multi-sine excitations, even if the overall SPL is the same, because the frequencies far from the resonance are not absorbed by the liner and thus counterbalance the high near-resonance absorption [18]. This specific behavior near resonance does not appear as clearly on the LEONAR sample, highlighting that the thermal behavior of this sample differs from the thermal behavior of the SDOF sample. This could be explained by the differences in the internal structure. Indeed, the thermocouple measurements made by Méry et al. [17] on the same SDOF sample showed that most of the temperature gradient occurs in the first few millimeters below the perforated plate; in the case of the LEONAR, the extended necks may change this temperature distribution inside the cavities, making the vortex shedding effect much less effective as the air is trapped in the space between the extended necks. A numerical investigation made by Yang et al. [25], where a conventional and an extended-tube liner were compared, has confirmed that in an extended-tube configuration such as the LEONAR sample, the vortices shed at the bottom of the tubes are indeed weaker than in the conventional case.

B. Influence of the direction of the thermal gradient

The thermal effects at the liner surface can also be described using the Biot number, Bi, instead of the temperature, as it allows easier comparisons between thermal configurations given its link to the convective heat transfer coefficient. The Biot number is defined by:

$$\mathrm{Bi} = \frac{L_s h}{k_{\mathrm{body}}} \tag{6}$$

where h is the convective heat transfer coefficient L_s is the sample's height (in the z direction) and k_{body} is the computed equivalent thermal conductivity of the sample.

In our setup, solving the 1D heat equation yields:

$$\mathrm{Bi} = \frac{T_b - T_u}{T_u - T_{flow}} \tag{7}$$

where T_b, T_u and T_{flow} are the temperatures of the backplate, the perforated plate and the grazing flow respectively.

When the coupling between acoustics and thermal effects is homogeneous on the whole liner surface, the averaged Biot number over the whole liner surface is a good description of the phenomena involved. As shown in Fig. 23, when acoustic excitation is applied , the averaged Biot number increases.As all other boundary conditions remain unchanged, this means that the heat convection increases at the surface of the sample. The increase is similar on both samples, even if the reference value is not the same due to a lower surface temperature on the LEONAR sample. The higher Biot numbers on the LEONAR sample are linked to its lower thermal conductivity compared to the SDOF sample.

Using the Biot number allows a direct comparison of different thermal configurations, as it eliminates the influence

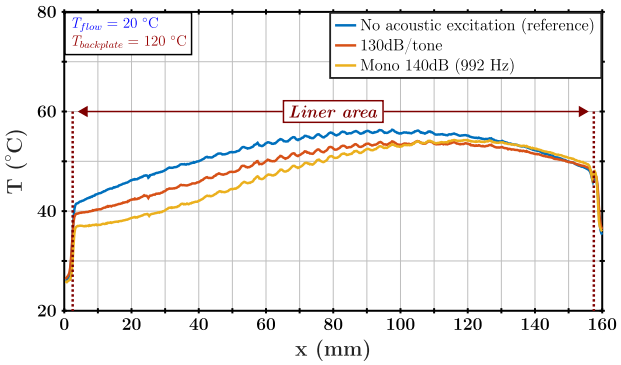

Fig. 19 Sample SDOF, q_m = 50 g/s, ΔT=+100 K, different sound excitations, streamwise profile.

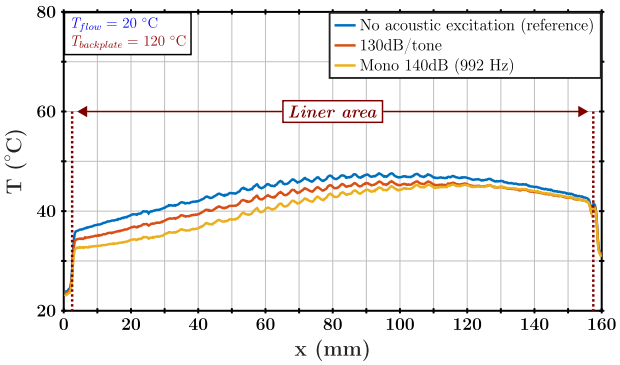

Fig. 20 SDOF, q_m = 100 g/s, ΔT=+100 K, different sound excitations, streamwise profile.

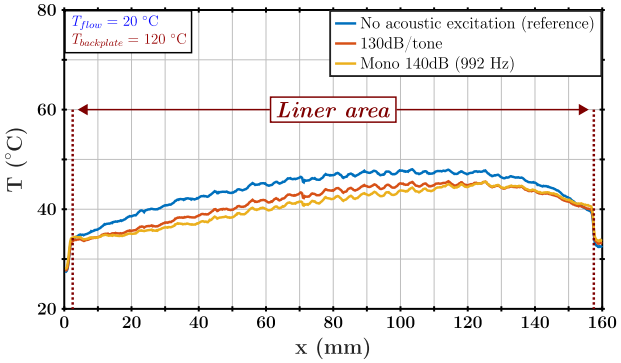

Fig. 21 Sample LEONAR, q_m = 50 g/s, ΔT=+100 K, different sound excitations, streamwise profile.

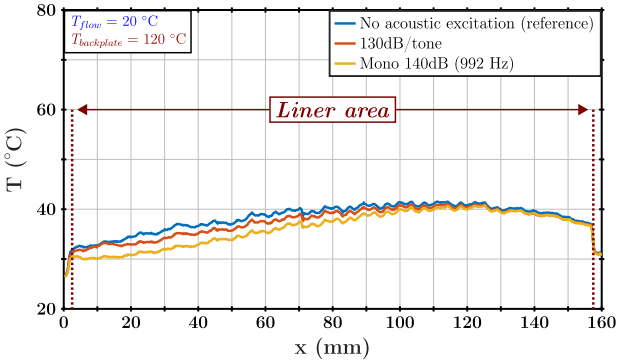

Fig. 22 LEONAR, q_m = 100 g/s, ΔT=+100 K, different sound excitations, streamwise profile.

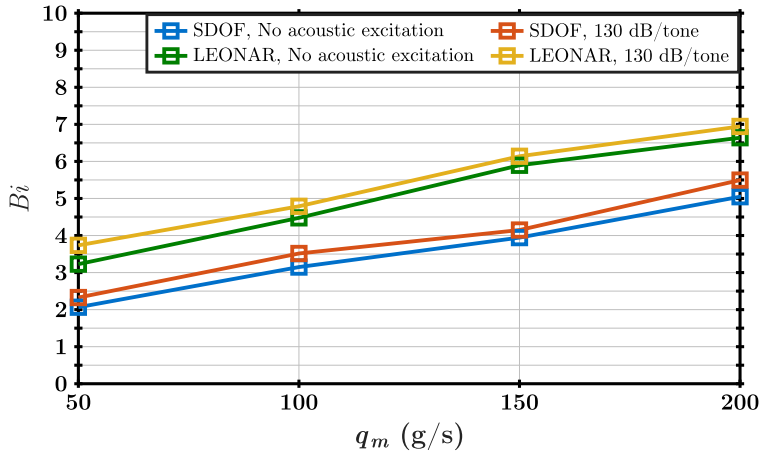

Fig. 23 Biot number (averaged over the whole surface) as a function of q_m, comparison between reference value and with acoustic excitation of SPL=130 dB/tone for each sample, ΔT=+100 K.

of the sign of the thermal gap ΔT: Bi is always positive and increases with h no matter the actual temperature of the flow. Table 4 presents the values of Bi obtained on both samples, as well as the absolute and relative variations ΔBi and $\Delta \mathrm{Bi}/\mathrm{Bi}_{ref}$, at several flow speeds and different thermal gradient values. For both samples, ΔBi decreases when q_m increases, no matter the value of ΔT; this confirms that the grazing flow dominates the coupling effect at higher flow

speeds. At a given flow speed, the values of the Biot number are identical when $\Delta T = +70$ K and when $\Delta T = +100$ K. The same result can be observed in cases with $\Delta T < 0$. This suggests that the value and direction of the gradient have little impact on the intensity of the coupling between thermal and acoustic effects.

The slight discrepancy between the values of the Biot number for positive and negative thermal gradient configurations at the same flow rate is explained by the differences between the experimental setups. Indeed, the experiments used flow rate as the reference , but it is in fact the Mach number M_b that is linked to the intensity of the flow and thus to the intensity of the coupling. Since M_b is higher in negative configurations due to the higher flow temperature, the flow effect is stronger and thus the increase of Bi is lower than in the equivalent (in terms of flow rate) positive configurations. Moreover, in the positive case, the bottom of the liner is heated but the rest of the test section remainds at ambient temperature, while in the negative case the whole duct heats up with the flow; the convective effects are thus different. Figure 24 presents the data from the last column of Table 4, plotted as a function of the Mach number instead of the flow rate to illustrate this effect. Apart from the measurements at $q_m = 150$ g/s which appear to be off, the general behavior is consistent regardless of the thermal configuration, and the observed differences between negative and positive gradients indeed seem to be linked to the increase of M_b in negative thermal configurations. There is a clear gap between the behavior at low flow speeds (M_b smaller than 0.1) and at higher flow speeds; this gap confirms that the coupling between thermal and acoustic effects is competing with the grazing flow effect. This competition between the influences of high SPL and high flow speeds has been previously studied [24]: it was found that for Mach numbers lower than 0.1, the acoustic effects dominate, but are gradually overwhelmed by the grazing flow until they become too small to be captured.

Table 4 Biot number evolution for different thermal conditions on both samples. Bi is averaged over the whole liner surface.

Sample	q_m (g/s)	ΔT	M_b	$\mathrm{Bi}_{\mathrm{ref}}$	Bi_{130}	$\Delta\mathrm{Bi}$	$\Delta\mathrm{Bi}/\mathrm{Bi}_{\mathrm{ref}}$
SDOF	50	+100	0.048	2.15	2.59	0.44	20.5%
		+70		2.15	2.61	0.46	21.4%
		-70	0.054	1.6	1.87	0.27	16.9%
		-100	0.056	1.57	1.83	0.25	16.9%
	100	+100	0.097	3.14	3.52	0.37	11.8%
		-100	0.112	2.55	2.71	0.16	6.3%
	150	+100	0.145	3.94	4.15	0.21	5.1%
	200	+100	0.194	5.04	5.49	0.45	8.9%
	260	+100	0.251	6.19	6.39	0.2	3.2%
		-100	0.290	5.8	5.87	0.07	1.2%
LEONAR	50	+100	0.048	3.16	3.7	0.54	17.1%
		+70		3.12	3.76	0.64	20.5%
	100	+100	0.097	4.68	4.95	0.27	5.8%
		+70		4.43	4.69	0.26	5.9%
	150	+100	0.145	5.89	6.14	0.25	4.2%
	200	+100	0.194	6.63	6.94	0.31	4.7%

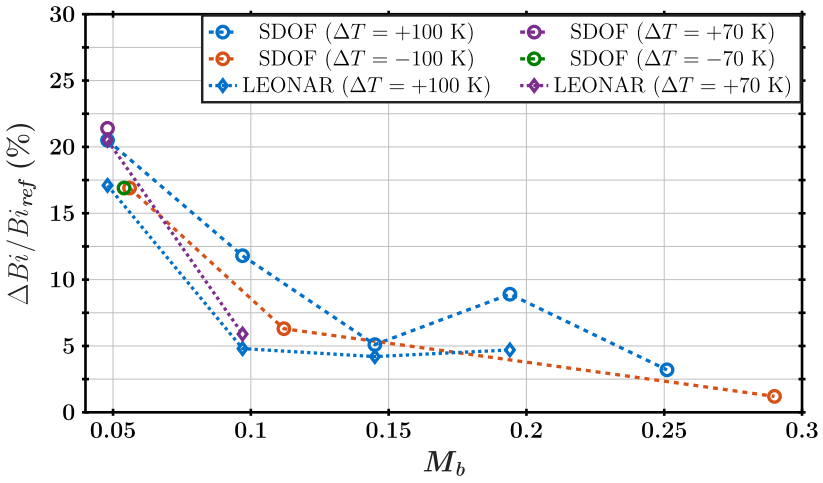

Fig. 24 Relative variations of the Biot number as a function of M_b, comparison between the two samples in different thermal configurations. SPL set to 130 dB/tone.

V. Conclusion

The behavior of two different types of liners under the influence of grazing flow, high SPL and thermal gradients has been studied using infrared thermography. Both liners were designed to have very similar acoustic characteristics, from an impedance perspective, even though their internal structures differ significantly. Thus, their acoustic behaviors, characterized using a classical impedance eduction method, are very similar. A specific experimental setup allowed for the creation of precise thermal gradients and measurements of the samples' surface temperature with infrared thermography. The influence of these thermal gradients on the impedance of the samples was found to be small, but a coupling between high acoustic levels and the surface temperature of liners was shown. This aerothermal coupling with the acoustic behavior of the liner effect is linked to an increase in the heat convection at the surface of the liner caused by the incident acoustic waves. Hence, the Biot number, Bi, was used to describe such coupling and compare the behaviors of different liners in various conditions. The flow speed seems to be the main driving parameter for the intensity of the coupling: the additional heat convection effect is high at low flow rates but is reduced for higher flow rates due to the grazing flow effect overwhelming the acoustic level effect. This behavior is similar on both samples when the acoustic excitations are multi-tone , and the existence and intensity of the coupling turn out to be independent of the actual value and direction of the thermal gradient between the sample's top and bottom. The coupling effect observed is thus clearly linked to the acoustic behavior of the liners, which explains the competition with the influence of the grazing flow. Near the acoustic resonance, the aerothermal coupling with the acoustic behavior of the liner effect becomes spatially localized; this is mainly linked to the structure and behavior of the sample with respect to high incident SPL. It appears mostly on the SDOF sample which might be less linear than the LEONAR concept regarding SPL effects. The hlrevAaerothermal coupling with the acoustic behavior of the liner effect observed on these two samples is still smaller than the coupling that would appear on SDOF samples with thin facesheets, which are even more nonlinear with respect to incident SPL [18]. The LEONAR sample is attractive in the context of the UHBR since its acoustic behavior is similar to the equivalent SDOF sample and takes less volume and mass. Moreover, this study showed that the surface temperature of the LEONAR sample is less affected by incident acoustic waves near the acoustic resonance due to its specific internal structure.

Acknowledgments

The work presented in this paper has been funded by Région Occitanie. The authors thank Delphine Sebbane and Nicolas Fasano for designing and helping with the experimental setup, as well as Philippe Reulet and Thomas Batmalle for helping during the infrared measurements. Rémi Roncen is warmly acknowledged for his help on the impedance eduction part. Jeanne Methel is warmly acknowledged for the English review.

References

[1] Motsinger, R. E., and Kraft, R. E., "Design and performance of duct acoustic treatment," *Aeroacoustics of Flight Vehicles: Theory and Practice. Volume 2: Noise Control*, 1991.

[2] Zhang, Q., and Bodony, D. J., "Numerical investigation of a honeycomb liner grazed by laminar and turbulent boundary layers," *Journal of Fluid Mechanics*, Vol. 792, 2016, pp. 936–980. https://doi.org/https://doi.org/10.1017/jfm.2016.79.

[3] Guess, A. W., "Calculation of perforated plate liner parameters from specified acoustic resistance and reactance," *Journal of Sound and Vibration*, Vol. 40, No. 1, 1975, pp. 119–137. https://doi.org/10.1016/S0022-460X(75)80234-3, URL http://www.sciencedirect.com/science/article/pii/S0022460X75802343.

[4] Ingård, U., and Labate, S., "Acoustic circulation effects and the nonlinear impedance of orifices," *The Journal of the Acoustical Society of America*, Vol. 22, No. 2, 1950, pp. 211–218. https://doi.org/10.1121/1.1906591.

[5] Ingård, U., and Ising, H., "Acoustic nonlinearity of an orifice," *The journal of the Acoustical Society of America*, Vol. 42, No. 1, 1967, pp. 6–17. https://doi.org/10.1121/1.1910576.

[6] Selamet, A., and Lee, I., "Helmholtz resonator with extended neck," *The Journal of the Acoustical Society of America*, Vol. 113, No. 4, 2003, pp. 1975–1985. https://doi.org/10.1121/1.1558379.

[7] Simon, F., "Long elastic open neck acoustic resonator for low frequency absorption," *Journal of Sound and Vibration*, Vol. 421, 2018, pp. 1–16. https://doi.org/10.1016/j.jsv.2018.01.044.

[8] Simon, F., Mery, F., Roncen, R., Sebbane, D., Piot, E., Davoine, C., and Thomas, M., "Overview of low frequency resonators based on LEONAR design," *INTER-NOISE and NOISE-CON Congress and Conference Proceedings*, Vol. 262, Institute of Noise Control Engineering, 2020, pp. 423–430.

[9] Guo, J., Fang, Y., Jiang, Z., and Zhang, X., "An investigation on noise attenuation by acoustic liner constructed by Helmholtz resonators with extended necks," *The Journal of the Acoustical Society of America*, Vol. 149, No. 1, 2021, pp. 70–81. https://doi.org/10.1121/10.0002990.

[10] Guo, J., Zhou, T., Fang, Y., and Zhang, X., "Experimental study on a compact lined circular duct for small-scale propeller noise reduction," *Applied Acoustics*, Vol. 179, 2021, p. 108062. https://doi.org/10.1016/j.apacoust.2021.108062, URL https://www.sciencedirect.com/science/article/pii/S0003682X21001559.

[11] Elnady, T., Bodén, H., and Kontio, T., "Impedance of SDOF perforated liners at high temperatures," *10^{th} AIAA/CEAS Aeroacoustics Conference*, 2004, p. 2842.

[12] Howerton, B., and Jones, M., "A Conventional Liner Acoustic/Drag Interaction Benchmark Database," *23^{rd} AIAA/CEAS Aeroacoustics Conference*, 2017. https://doi.org/https://doi.org/10.2514/6.2017-4190.

[13] Jasinski, C., and Corke, T., "Mechanism for Increased Viscous Drag over Porous Sheet Acoustic Liners," *AIAA Journal*, Vol. 58, No. 8, 2020, pp. 3393–3404. https://doi.org/10.2514/1.J059039.

[14] Léon, O., Méry, F., Piot, E., and Conte, C., "Near-wall aerodynamic response of an acoustic liner to harmonic excitation with grazing flow," *Experiments in Fluids*, Vol. 60, No. 9, 2019, p. 144. https://doi.org/10.1007/s00348-019-2791-5.

[15] Giachetti, B., Fénot, M., Couton, D., and Plourde, F., "Influence of multi-perforation synthetic jet configuration on heat transfer enhancement," *International Journal of Heat and Mass Transfer*, Vol. 125, 2018, pp. 262–273. https://doi.org/10.1016/j.ijheatmasstransfer.2018.04.073, URL http://www.sciencedirect.com/science/article/pii/S0017931017353425.

[16] Esnault, S., Duchaine, F., Gicquel, L., and Moreau, S., "Large Eddy Simulation of Heat Transfer Within a Multi-Perforation Synthetic Jets Configuration," *Journal of Turbomachinery*, Vol. 142, No. 6, 2020. https://doi.org/10.1115/1.4046545, 061010.

[17] Méry, F., Piot, E., Sebbane, D., Reulet, P., Simon, F., and Carazo Méndez, A., "Experimental Assessment of the Effect of Temperature Gradient Across an Aeroacoustic Liner," *Journal of Aircraft*, Vol. 56, No. 5, 2019, pp. 1809–1821. https://doi.org/https://doi.org/10.2514/1.C035157.

[18] Lafont, V., Mery, F., Reulet, P., and Simon, F., "Surface temperature measurement of acoustic liners in the presence of grazing flow and thermal gradient," *Experiments in Fluids*, Vol. 62, 2021. https://doi.org/10.1007/s00348-021-03184-w.

[19] Roncen, R., Méry, F., Piot, E., and Simon, F., "Statistical Inference Method for Liner Impedance Eduction with a Shear Grazing Flow," *AIAA Journal*, Vol. 57, No. 3, 2019, pp. 1055–1065. https://doi.org/10.2514/1.J057559.

[20] Minotti, A., Simon, F., and Gantié, F., "Characterization of an acoustic liner by means of Laser Doppler Velocimetry in a subsonic flow," *Aerospace Science and Technology*, Vol. 12, No. 5, 2008, pp. 398–407. https://doi.org/10.1016/j.ast.2007.09.007, URL http://www.sciencedirect.com/science/article/pii/S1270963807001150.

[21] Colburn, A. P., "A method of correlating forced convection heat-transfer data and a comparison with fluid friction," *International Journal of Heat and Mass Transfer*, Vol. 7, No. 12, 1964, pp. 1359–1384. https://doi.org/10.1016/0017-9310(64)90125-5, URL https://www.sciencedirect.com/science/article/pii/0017931064901255.

[22] Chung, J. Y., and Blaser, D. A., "Transfer function method of measuring in-duct acoustic properties. I. Theory," *The Journal of the Acoustical Society of America*, Vol. 68, No. 3, 1980, pp. 907–913. https://doi.org/10.1121/1.384778.

[23] Primus, J., Piot, E., and Simon, F., "An adjoint-based method for liner impedance eduction: Validation and numerical investigation," *Journal of Sound and Vibration*, Vol. 332, No. 1, 2013, pp. 58–75. https://doi.org/https://doi.org/10.1016/j.jsv.2012.07.051, URL http://www.sciencedirect.com/science/article/pii/S0022460X12006268.

[24] Lafont, V., Méry, F., Roncen, R., Simon, F., and Piot, E., "Liner Impedance Eduction Under Shear Grazing Flow at a High Sound Pressure Level," *AIAA Journal*, Vol. 58, No. 3, 2020, pp. 1107–1117. https://doi.org/10.2514/1.J058756.

[25] Yang, C., Zhang, P., Jacob, S., Trigell, E., and Åbom, M., "Investigation of Extended-Tube Liners for Control of Low-Frequency Duct Noise," *AIAA Journal*, Vol. 59, No. 10, 2021, pp. 4179–4194. https://doi.org/10.2514/1.J059988.